J Mater Sci (2008) 43:6414–6421
DOI 10.1007/s10853-008-2718-7



# Spark plasma sintering of ultra refractory compounds

**Diletta Sciti · Mats Nygren**

Received: 23 November 2007 / Accepted: 12 May 2008 / Published online: 30 July 2008


**Abstract** Spark plasma sintering experiments were conducted on Zr- and Hf-based borides and carbides with the addition of 1, 3, and 9 vol% $MoSi_2$ as sintering aid. For comparison, as-received ZrC, HfC, $ZrB_2$, $HfB_2$ powders were also sintered. The microstructural features were investigated by means of scanning electron microscop–energy dispersive spectroscopy technique. Silicon carbide was detected in all the doped compositions along with significant amounts of oxide species (Hf/$ZrO_2$, and $SiO_2$). The effect of the $MoSi_2$ content on densification, microstructure, and mechanical properties is analyzed.

## Introduction

Spark plasma sintering (SPS) is a newly developed pressure sintering process that makes use of a pulsed DC current to heat the sample. The SPS process allows to sinter and sinter-bond materials at lower temperatures and in a shorter time than in conventional sintering. The use of a pulsed DC current is said to have a surface-activating and cleaning effect on the particles being sintered. Higher densities, refined microstructures, clean grain boundaries and elimination of surface impurities have been reported in the literature for several ceramic materials densified by SPS, as well as an overall improvement in the materials performance [1–7]. Additional advantages include ease of operation and accurate control of the sintering energy as well as rapid sintering speed, high reproducibility, safety, and reliability [1–7]. Therefore this technique is particularly attractive for industrial applications of poorly sinterable materials that are difficult to fabricate by conventional sintering techniques. Borides, carbides, and nitrides are all typically difficult to densify because of their covalent bonding characteristics. Therefore, techniques such as SPS are attractive to reduce sintering temperatures and to enhance their mechanical properties through improved densification and microstructure control.

In this contribution sintering experiments are carried out for carbides and borides of zirconium and hafnium that are notorious for their poor sinterability [8–14]. The interest in these compounds derives from a combination of important engineering properties such as high melting points (>3,200 °C), high hardness, solid-state stability, good thermochemical and thermomechanical properties [8–14].

The aim of this work is to exploit the potential of the SPS technique, attempting the densification of these compounds with as little sintering aid as possible. $MoSi_2$ is selected as sintering additive as it has been previously shown that in higher concentrations than those of the present work it improves the densification and the mechanical properties of these refractory compounds [15–17]. Compositions with 1, 3, and 9 vol% $MoSi_2$ are produced. For the sake of comparison, the densification of undoped starting powders is also attempted. The sinterability of these powders and the microstructure of densified compacts are studied as a function of the sintering aid amount added and compared to the microstructures of the undoped materials.

D. Sciti (✉)
ISTEC-CNR, Institute for Science and Technology of Ceramics,
Via Granarolo 64, 48018 Faenza, Italy
e-mail: dile@istec.cnr.it

M. Nygren
Arrhenius Laboratory, Department of Inorganic Chemistry,
Stockolm University, 10691 Stockolm, Sweden

## Experimental

Commercial powders were used to prepare the ceramic materials: $ZrB_2$ Grade B (H. C. Starck, Germany), mean particle size $\approx$2 μm; $HfB_2$ (Cerac Incorporated, Milwaukee, USA), −325 mesh, mean particle size $\approx$1 μm; ZrC Grade B (H. C. Starck, Germany), mean particle size $\approx$3.8 μm, HfC (Cerac Inc., Milwaukee, WI), −325 mesh, mean particle size 0.8 μm; $MoSi_2$ <2 μm (Aldrich, Milwaukee, USA), mean particle size $\approx$2.8 μm.

The following compositions were prepared:

$ZrB_2$ + (0, 1, 3, 9) vol% $MoSi_2$ labeled as ZB0, ZB1, ZB3, ZB9, respectively.
$HfB_2$ + (0, 1, 3, 9) vol% $MoSi_2$ labeled as HB0, HB1, HB3, HB9, respectively.
ZrC + (0, 1, 3, 9) vol% $MoSi_2$ labeled as ZC0, ZC1, ZC3, ZC9, respectively.
HfC + (0, 1, 3, 9) vol% $MoSi_2$ labeled as HC0, HC1, HC3, HC9, respectively.

The powder mixtures were ultrasonically treated and ball-milled for 24 h in absolute ethanol using zirconia milling media, which subsequently dried in a rotary evaporator and sieved through a 60-μm-mesh screen size. For sintering tests of monolithic materials, raw powders were ultrasonically treated to eliminate agglomerates and milled using zirconia milling media. Doped and undoped powders were sintered in a graphite mold using an SPS furnace (Dr Sinter 2050, Syntec Inc., Kanagawa, Japan). A double layer of graphite blanket was placed around the die in order to minimize heat loss. The temperature was measured by an optical pyrometer focused on the graphite die. The sintered pellets were 12 mm in diameter and 5 mm in height. For $MoSi_2$-doped powders, the sintering cycle was adopted as follows. From room temperature up to 600 °C the heating rate was set at 300 °C/min. At 600 °C, a pressure of 100 MPa was applied and the temperature was then raised to 1,400 °C using a heating rate of 200 °C/min. From 1,400 °C to the final sintering temperature (1,700–1,900 °C) the heating rate was decreased to 100 °C/min. Holding times were 3–5 min. For undoped powders the applied pressure was decreased to 65 MPa for HfC and $HfB_2$ and 75 MPa for ZrC and $ZrB_2$. The vacuum level ranged typically from 5 at low temperatures to 10 Pa at high temperatures.

Bulk densities were measured by the Archimedes method. Relative densities were determined as the ratio between bulk and theoretical densities calculated on the basis of starting nominal compositions using the rule of mixtures. Crystalline phases were identified by X-ray diffraction (Siemens D500, Karlsruhe, Germany). The microstructures were analyzed using scanning electron microscopy (SEM, Cambridge S360, Cambridge, UK) and energy dispersive spectroscopy (EDS, INCA Energy 300, Oxford instruments, UK). Microstructural parameters were determined through image analysis on SEM micrographs of polished surfaces using a commercial software program (Image Pro-plus 4.5.1, Media Cybernetics, Silver Springs, MD, USA). Vickers microhardness (HV1.0) was measured with a load of 9.81 N, using a Zwick 3212 tester (Zwick, Ulm, Germany). Eight to ten indentations were made for each sample. Fracture toughness ($K_{Ic}$) was evaluated by the direct crack measurement (DCM), by using the equation of Anstis et al. [18]. Five indentations were performed in each sample.

## Results and discussion

### Sintering tests

Different conditions of holding time, applied pressure, and temperatures were tested in order to get the highest densities. The maximum temperature was set on the basis of the dilatometer reading, i.e., when increasing the temperature did not yield further shrinkage of the powder compact. It must be clarified that the sintering temperatures recorded on the external wall of the graphite die are certainly underestimated with respect to the temperatures, the specimens are exposed to during sintering. Extensive studies on the SPS process have demonstrated that for conductive materials, like those of the present work, the actual temperature inside the specimens is significantly higher than on the external wall of the die where the pyrometer is focused [7]. The temperature mismatch depends on many factors such as the size of the die, the quality of the vacuum, the level of insulation of the die, thermal and electrical conductivity of the die, etc. Under the present conditions the temperature mismatch was estimated to be in the range 100–125 up to 1,700 °C. Indeed, according to previous experiments, alumina, which melts around 2,070 °C, was sintered at 1,850 °C without any feature of being melted, suggesting that the temperature mismatch at this temperature is $\leq$200 °C. However, this mismatch increases with increasing temperature and it is likely that in the range of 1,900–2,200 °C it might be about 250 °C, in agreement with previous results [7].

Under proper setting of the sintering conditions, densities in excess of 97% were obtained for all the composite and monolithic materials, with the sole exception of undoped $HfB_2$ (Table 1). As-received $ZrB_2$ and ZrC powders were sintered to 98–99% of final relative density at 2,100 °C (i.e., at a true temperature >2,300 °C), HfC was densified to 98% at 2,200 °C (i.e., >2,400 °C). $HfB_2$ only reached a final density of 80% despite several attempts at temperatures higher than 2,300 °C.

**Table 1** Compositions, sintering parameters, and relevant microstructural parameters of the borides and carbides prepared

| Borides | | | | | | Carbides | | | | | |
|---|---|---|---|---|---|---|---|---|---|---|---|
| Sample | *T*/*t* (°C/min) | *D* (%) | MGS (μm) | SiC (vol%) | Residual $MoSi_2$ (vol%) | Sample | *T*/*t* (°C/min) | *D* (%) | MGS (μm) | SiC (vol%) | Residual $MoSi_2$ (vol%) |
| ZB0 | 2,100/3 | 98 | 25 | – | – | ZC0 | 2,100/3 | 99 | 13 | – | – |
| ZB1 | 1,850/5 | 98 | 4 | 0.5 | Traces | ZC1 | 1,950/3 | 99 | 7 | 2 | Traces |
| ZB3 | 1,750/3 | 100 | 2 | 1 | Traces | ZC3 | 1,900/3 | 99 | 6 | 4 | Traces |
| ZB9 | 1,700/5 | 100 | 2 | 1 | ~8 | ZC9 | 1,700/3 | 99 | 4 | 5 | 6–7 |
| HB0 | 2,200/5 | 80 | 10 | – | – | HC0 | 2,200/3 | 98 | 19 | – | – |
| HB1 | 1,750/3 | 97 | 1 | 1 | <0.5 | HC1 | 1,900/5 | 98 | 2 | 1.5 | <0.5 |
| HB3 | 1,750/3 | 99 | 1 | 1 | ~1 | HC3 | 1,750/5 | 100 | 1 | 2 | <0.5 |
| HB9 | 1,750/3 | 99 | 1 | 1 | ~8 | HC9 | 1,750/5 | 99 | 1 | 1.5 | ~8 |

*T*, sintering temperature; *t*, dwelling time; *D*, relative density; MGS, mean grain size

The addition of $MoSi_2$ enhanced the densification of the composites even in amounts of 1 vol%. Typical shrinkage and shrinkage rate curves are shown in Fig. 1, for the HB1 mixture sintered at 1,800 °C. For compositions with 1 vol% additions densities in excess of 97–98% were obtained at temperature 200–300 °C lower than those necessary for undoped powders. Further increase in $MoSi_2$ content generally led to decrease in the sintering temperature. For composites with 9% $MoSi_2$, the maximum temperatures were 400–450 °C lower than those needed for undoped powders. The reduction of the sintering temperature also led to a marked refinement of the microstructure (Table 1), as illustrated below. No relationship could be established between mean grain size of sintered materials and variation of the holding time between 3 and 5 min (Table 1).

## Microstructural features

### *$ZrB_2$-based materials*

According to the X-ray diffraction studies, the crystalline phases detected in 9% doping level compositions (ZB9) were hexagonal $ZrB_2$ and tetragonal $MoSi_2$ (Fig. 2). Traces of $MoSi_2$ phase were also recognizable in the diffraction spectra of the compositions with 3 vol% doping (ZB3). In compositions with 1% doping (ZB1), no diffraction peaks from $MoSi_2$ were detected.

Monolithic $ZrB_2$ (Fig. 3a) is characterized by globular grains with the dimensions of the order of 25 μm and an evenly distributed porosity (2%). A low level of porosity is also present in the composition with 1% $MoSi_2$ (ZB1,

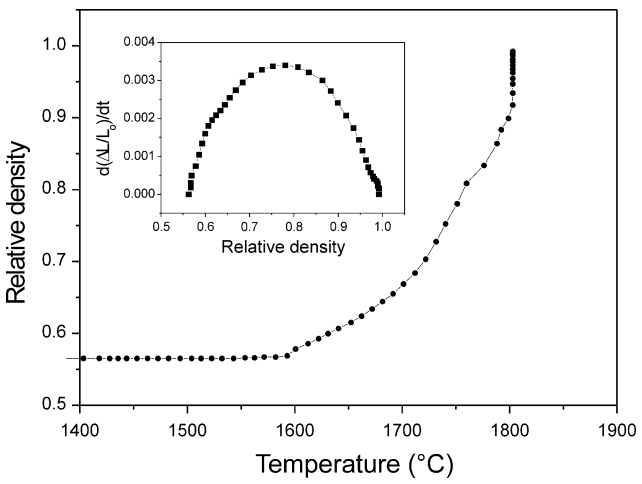


**Fig. 1** The relative density and shrinkage rate recorded during sintering of the composition $HfB_2$ + 1 vol% $MoSi_2$ (HB1). In the range 1,400–1,800 °C the heating rate is 100 °C/min

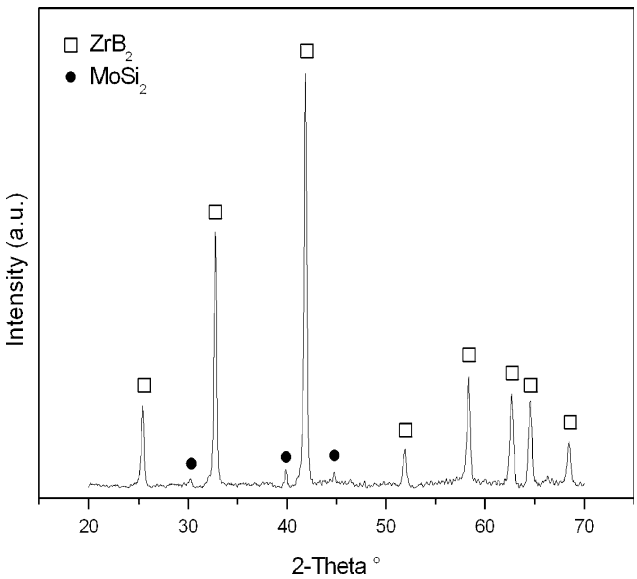


**Fig. 2** X-ray diffraction spectrum of the $ZrB_2$ + 9 vol% $MoSi_2$ (ZB9) sintered at 1,700 °C

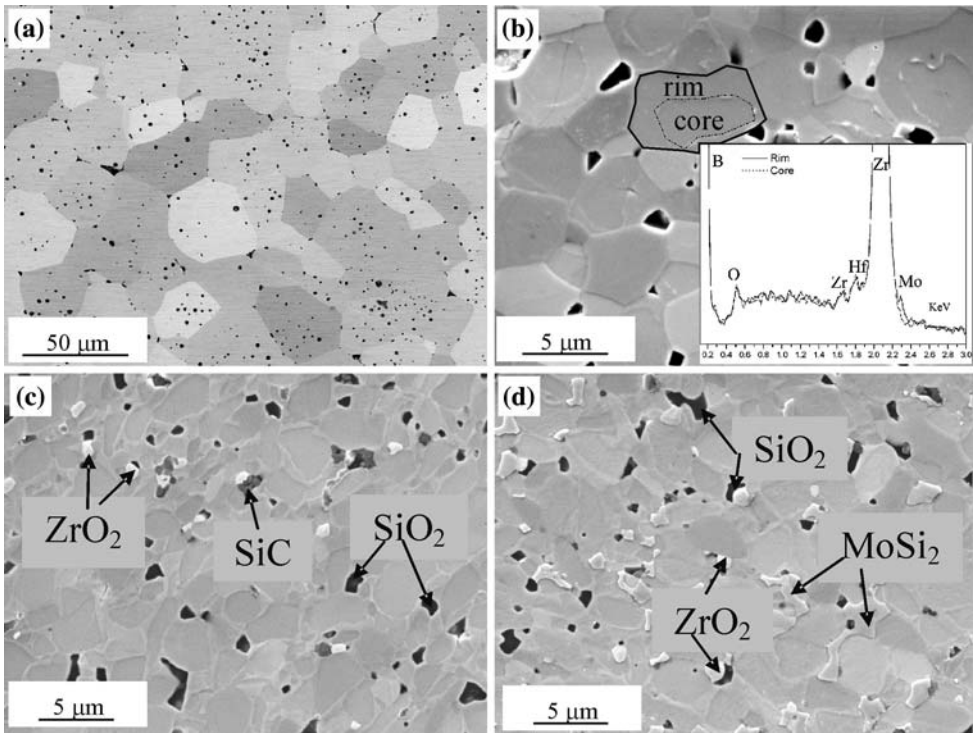


**Fig. 3** Polished sections of $ZrB_2$-based compositions; (**a**) ZB0, (**b**) ZB1 and EDS spectra of the core-rim structure of $ZrB_2$ grains, (**c**) ZB3, (**d**) ZB9

sintering at 1,850 °C, Fig. 3b), but the mean grain size is notably reduced to 4 μm (see Table 1). No porosity was detected on ZB3 sample sintered at 1,750 °C and ZB9 sample sintered at 1,700 °C (Fig. 3c, d) and both compositions have fine-grained microstructure with $ZrB_2$ grain sizes comparable to those of the starting boride powder. Common features for these $ZrB_2$-based composites are the presence of oxide phases such as silica and zirconia, and traces of SiC. The presence of silica can be attributed to the $SiO_2$ coating of the starting $MoSi_2$ powder particles. Zirconia could derive both from oxygen contamination of the starting $ZrB_2$ powder and from the milling media. Small SiC grains were generally observed to form associated with the silica pockets and their formation accounts for C contamination. Carbon impurities are found in the starting $ZrB_2$ powder. Further Carbon sources are the polyethylene bottles used for ball milling and the graphite-rich sintering environment. $ZrB_2$ grains were found to have a sub-structure, resembling a core-shell structure (Fig. 3b). By EDS analysis pure $ZrB_2$ phase was recognized in the cores, while Zr, B, and small amounts of Mo were detected in the shell (see EDS spectrum). The latter phase was recognized as a $(Zr,Mo)B_2$ solid solution, in agreements with previous findings on pressureless-sintered materials with the addition of either Mo or $MoSi_2$ [17, 19].

*$HFB_2$-based materials*

Similar to $ZrB_2$-based samples, the X-ray diffraction patterns of the $HfB_2$-based composites only contained reflections that could be ascribed to $HfB_2$ but pattern of the composition with 9% $MoSi_2$ analysis did contain a few reflections of low intensity originating from $MoSi_2$. The fracture surface of HB0 (Fig. 4a) shows that residual porosity and grain coarsening are the main features that characterize this monolithic material. The mean grain size was of the order of 10 μm, i.e., one order of magnitude larger than that of the starting powder particles. The combination of these two features suggests that a non-densifying vapor phase transport mechanism may be dominant at this temperature. Further tests are in progress in order to improve the final relative density.

Little or no porosity was generally found in the $MoSi_2$-containing composites which all exhibited very fine-grained microstructures (see Table 1 and Fig. 4b–d). No grain growth occurred for these compositions as the resulting mean grain size is about 1 μm, i.e., close to that of the starting particles of the $HfB_2$ powder. The $MoSi_2$ phase has an irregular shape and is accommodated among the voids generated by the diboride skeleton. A considerable quantity of $HfO_2$ (4 vol%) was detected by EDS analysis, which accounts for oxygen contamination of the starting powder. Small amounts of $SiO_2$ (0.5%) and SiC (1%) were also detected. Silicon carbide was found to form preferentially at $MoSi_2$ sites. Traces of Mo were found inside $HfB_2$ grains, suggesting that a core-rim structure could have formed, similar to $ZrB_2$-based materials (Fig. 4c).

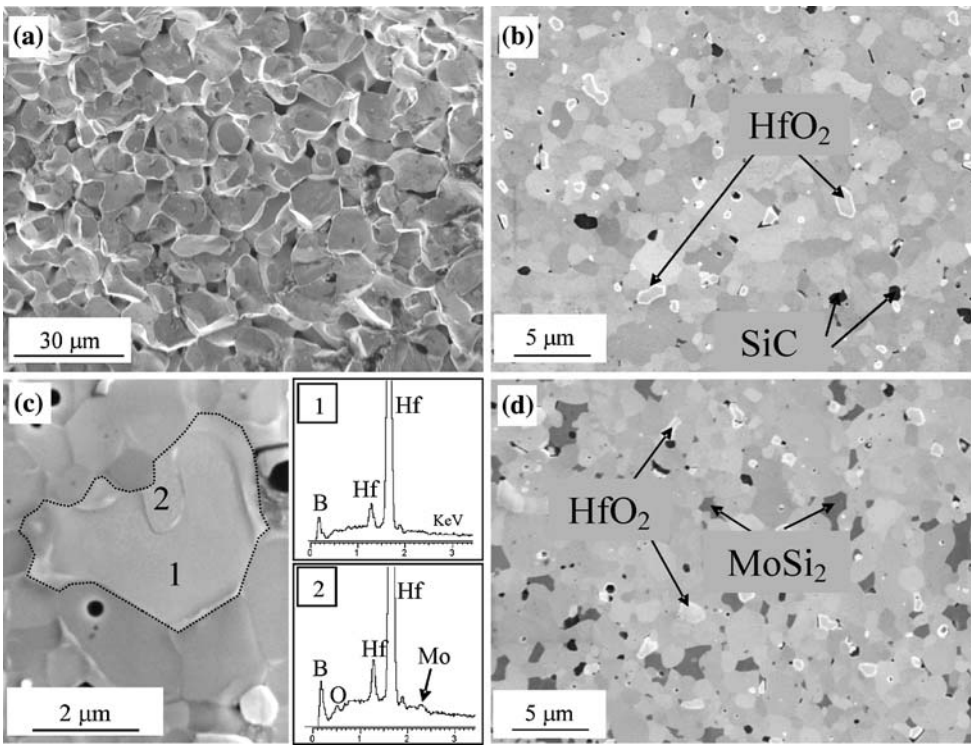


**Fig. 4** $HfB_2$-based compositions. (**a**) Fracture surface of porous HB0, (**b**) Polished surface of HB1, (**c**) Polished surface of HB3 and EDS spectra showing traces of Mo inside an $HfB_2$ grain, (**d**) Polished surface of HB9

*ZrC-based materials*

The X-ray diffraction pattern of the composition with 9% $MoSi_2$ analysis did contain reflection from cubic ZrC, a few reflections of low intensity originating from $MoSi_2$, and traces of SiC. In the patterns of compositions with 1, 3% $MoSi_2$, reflections from ZrC were only detected. The polished section of Z0 is shown in Fig. 5a. Little or no porosity is found in the microstructure of this material. The black contrasting features were recognized as carbon by EDS analysis and were attributed to the free carbon impurities present in the starting ZrC powder. The mean grain size of Z0 is 13 μm. No porosity was found in the microstructure of Z1, sintered at 1,950 °C (Fig. 5b). Black contrasting features belong to residual carbon, as found in the microstructure of Z0. Furthermore reaction phases recognized as SiC and ZrSi or ZrSiC were also detected as small agglomerates of particles. Formation of these Si-phases is mainly due to $MoSi_2$ reaction with C or ZrC. Due to the low residual amount of the sintering additive, it was not possible to detect $MoSi_2$ in the microstructure of Z1. Similar features were displayed by the compositions with 3% of $MoSi_2$ (Fig. 5c). SiC particles were clearly detected in the microstructure of the ZC9 composition, while the determination of Zr–Si phase is uncertain (Fig. 5d). $MoSi_2$ is frequently detected along ZrC grain boundaries, forming phases with very low dihedral angles. These microstructural features suggest that $MoSi_2$ induces formation of liquid phases that work as medium for mass transfer mechanism, thus enhancing the densification. Small particles recognized as Zr–oxide phase were occasionally detected in the composites.

*HfC-based materials*

According to X-ray diffraction analysis, all the materials contained cubic HfC. Traces of tetragonal $MoSi_2$ were only found in the composition with 9 vol% $MoSi_2$. The main diffraction peak of $\beta$-SiC was also recognized in the spectrum of the HC3 composition. The polished section of HC0 is shown in Fig. 6a. The high temperature required for densification of this compound caused a notable coarsening of the microstructure, with the mean grain size increasing from the starting powder particle dimensions of <1 to ~20 μm (Table 1). A small amount of porosity, mainly trapped within the grains, is also evident.

The polished sections of the doped compositions are shown in Fig. 6b–d. A small amount of residual porosity and a refinement of the microstructure (mean grain size 2 μm) are apparent for HC1 (see Fig. 6b). No $MoSi_2$ was detected in this sample. Instead a minor amount of SiC was found. HC3 (data not shown) and HC9 compositions (Fig. 6c, d) were completely dense and in both cases the mean grain size was <1 μm. As for HC1, 1–2 vol% of SiC was detected in these microstructures. It is evident from Fig. 6d that SiC starts to form the site where $MoSi_2$ resides. Furthermore, the morphology of $MoSi_2$ suggests a liquid phase behavior during sintering, as for ZrC composites.

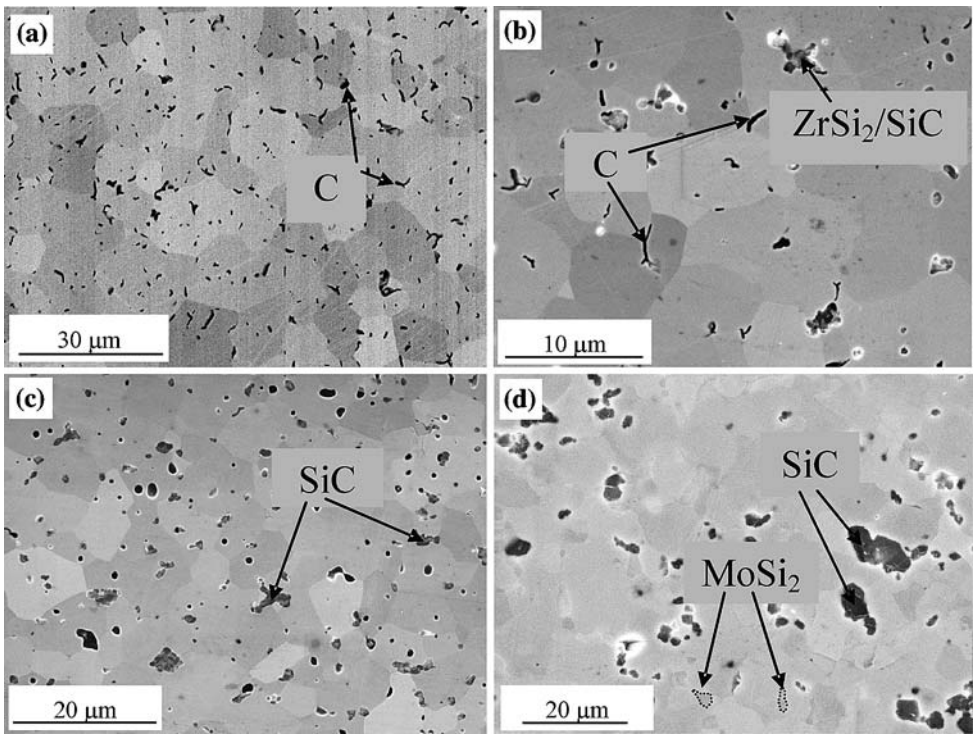


**Fig. 5** Polished sections of ZrC materials: (**a**) ZC0, (**b**) ZC1, (**c**) ZC3, (**d**) ZC9

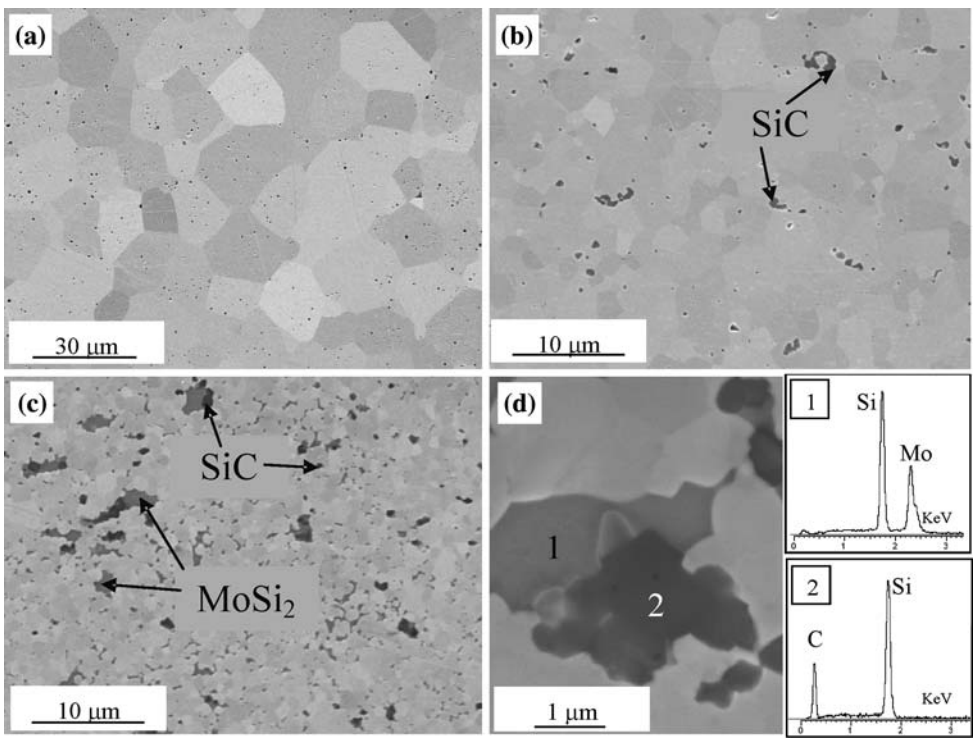


**Fig. 6** Polished sections of HfC materials: (**a**) HC0, (**b**) HC1, (**c**) HC9, (**d**) SiC formation at $MoSi_2$ site in HC9 and related EDS spectra

Traces of Hafnium oxide phase were occasionally detected in the composites.

Despite the obvious differences among the four systems investigated, it is also apparent that some similarities do occur. All composites contain substantial amounts of "impurity phases" such as $SiO_2$, SiC, and $Hf(Zr)O_2$. The origin of these oxides can in part be ascribed to impurities present in the starting powders and in part to partial decomposition of the added $MoSi_2$. In vacuum sintering with graphite heating elements, carbon monoxide strongly interacts with the materials under sintering causing carbothermal reduction of oxides and/or carburization of metals

[20]. Interaction of CO with $MoSi_2$ (at pressure of 10 Pa) leads to SiC formation at $T < 1{,}850$ °C and to decomposition of $MoSi_2$ at $T > 1{,}850$ °C. Furthermore the carbides can also work as carbon sources as they can have variable carbon content. Indeed, ZrC- and HfC-doped samples contain a larger amount of SiC and lower amounts of oxides than the borides. On the other hand, EDS studies show that in most samples Mo is lacking. Only in one case it was possible to experimentally verify that Mo entered the lattice of $ZrB_2$. Some evidence of molybdenum entering the lattice of $HfB_2$ was also found. Recently, it was reported that Mo has a significant solubility in ZrC (from 1.1 mol% at 1,800 °C to 9.4 mol% at 2,100 °C) [21]. It is very likely that Mo forms solid solutions even with the Hf- and Zr-carbides.

## Mechanical properties

Hardness and toughness values are summarized in Table 2. The hardness of the $ZrB_2$-based materials shows an initial small dependence on the $MoSi_2$ content as it slightly increases when $MoSi_2$ content is increased from 0 to 3 vol%. This is related to the concurrent decrease in mean grain size and residual porosity (Table 1). In contrast, ZB3 and ZB9 have the same value of hardness, ~18 GPa, despite the different starting $MoSi_2$ composition. Indeed these materials have similar values of mean grain size and density which are the most important factors affecting the hardness [22]. The hardness of $HfB_2$-based materials is not sensitive to the change of $MoSi_2$ content, as HB1, HB3, and HB9 have almost the same values. This is probably due to that the fact that the doped $HfB_2$-based compositions have similar values of mean grain size and density (see Table 1). The low hardness of the monolithic HB0 (7 GPa) is related to the high fraction of porosity. $HfB_2$-based compositions are harder than corresponding $ZrB_2$-ones, due to their finer microstructure. The hardness of ZrC-composites is not sensitive to the change of $MoSi_2$ content between 0 and 3 vol% (18–19 GPa). A slight increase is observed for the composition with 9% (20 GPa), very likely related to the refinement of the microstructure compared with the 0, 1, and 3%-doped compositions. The hardness of the HfC-based materials shows an initial dependence on the $MoSi_2$ content increasing when the initial $MoSi_2$ content is increased from 0 to 3 vol%. This is related to the concurrent decrease in mean grain size and residual porosity (Table 1). However, increasing the initial content of $MoSi_2$ to 9 vol% has no further effect on this property. HfC-based compositions are harder than corresponding ZrC-ones, due to their finer microstructure. Beside, in the investigated doping range, there is no substantial difference in microhardness between the $HfB_2$-based materials and the HfC-based materials.

Excessive spalling at the indentation sites prevented the measurement of fracture toughness by the DCM method in monolithic materials. The fracture toughness values are in agreement with those reported for similar materials, even if produced by different sintering techniques [15–17]. The highest toughness was found for the $HfB_2$ materials. For all the systems, there is an increase in toughness with the increase in the initial $MoSi_2$ content. These features suggest that when the $MoSi_2$ phase is retained in the microstructure a significant toughening mechanism can be activated, as for example that based on residual stresses [23]. Due to its high thermal expansion coefficient (8.5–9 $\times$ $10^{-6}$ $°C^{-1}$ [24]), $MoSi_2$ should generate compressive residual stress in the borides and carbides matrices (thermal expansion coefficients in the range (5.5–7.5 $\times$ $10^{-6}$ $°C^{-1}$ [24]), thus strengthening the microstructure.

## Conclusions

Ultra-refractory borides and carbides were densified by SPS with and without $MoSi_2$ as sintering aid. The addition of $MoSi_2$ enhanced the densification even in amounts as low as 1 vol%. Dense or nearly fully dense materials were obtained at temperatures around 300–400 °C lower than

**Table 2** Mechanical properties for selected borides and carbides

| Borides | | | Carbides | | |
|---|---|---|---|---|---|
| Sample | HV1.0 (GPa) | $K_{Ic}$ (MPa $m^{1/2}$) | Sample | HV1.0 (GPa) | $K_{Ic}$ (MPa $m^{1/2}$) |
| ZB0 | 15.6 ± 0.4 | – | ZC0 | 17.9 ± 0.6 | – |
| ZB1 | 16.5 ± 1.0 | 2.1 ± 0.1 | ZC1 | 18.8 ± 0.3 | 2.1 ± 0.2 |
| ZB3 | 18.3 ± 0.6 | 3.2 ± 0.1 | ZC3 | 18.4 ± 0.7 | 3.2 ± 0.4 |
| ZB9 | 18.2 ± 0.7 | 4.0 ± 0.6 | ZC9 | 20.0 ± 0.5 | 3.3 ± 0.4 |
| HB0 | 7.0 ± 0.4 | – | HC0 | 18.8 ± 0.7 | – |
| HB1 | 21.1 ± 0.6 | 4.4 ± 0.5 | HC1 | 20.2 ± 0.8 | 2.5 ± 0.1 |
| HB3 | 22.0 ± 0.6 | 4.5 ± 0.4 | HC3 | 21.8 ± 0.6 | 2.5 ± 0.1 |
| HB9 | 21.2 ± 0.9 | 4.9 ± 0.6 | HC9 | 21.1 ± 0.7 | 2.9 ± 0.6 |

those needed for the undoped materials with consequent refinement of the microstructure. In all the microstructures of the $MoSi_2$-doped materials, a small amount of SiC was detected.

Due to higher density and refined microstructure, the mechanical properties of the composites were generally higher than those of monolithic materials. The hardness was in the range 20–22 GPa for HfC and $HfB_2$ composites and 16–18 GPa for ZrC and $ZrB_2$ composites. The fracture toughness showed the tendency to increase with increasing the $MoSi_2$ content. The values of the doped $HfB_2$-based materials were in the range 4–5 MPa $m^{1/2}$.

**Acknowledgement** The authors wish to thank L. Silvestroni for materials preparation and G. Celotti for X-ray diffraction analysis.

## References

1. Shen Z, Zhao Z, Peng H, Nygren M (2002) Nature 417:266. doi:10.1038/417266a
2. Munir ZA, Anselmi-Tamburini U, Ohyanagi M (2006) J Mater Sci 41:763. doi:10.1007/s10853-006-6555-2
3. Nygren M, Shen Z (2004) Silic Indus 69:211
4. Groza JR, Zavaliangos A (2000) Mater Sci Eng A287:171. doi:10.1016/S0921-5093(00)00771-1
5. Groza JR, Garcia M, Schneider JA (2001) J Mater Res 16:286. doi:10.1557/JMR.2001.0043
6. Wang H, Wang CA, Yao X, Fang D (2007) J Am Ceram Soc 90:1992. doi:10.1111/j.1551-2916.2007.01665.x
7. Anselmi-Tamburini U, Kodera Y, Gasch M, Unuvar C, Munir ZA, Ohyanagi M, Johnson SM (2006) J Mater Sci 41:3097. doi:10.1007/s10853-005-2457-y
8. Fahrenholtz WG, Hilmas GE (2007) J Am Ceram Soc 90:1347. doi:10.1111/j.1551-2916.2007.01583.x
9. Upadhya K, Yang JM, Hoffmann WP (1997) Am Ceram Soc Bull 58:51
10. Opeka MM, Talmy IG, Wuchina EJ, Zaykoski JA, Causey SJ (1999) J Eur Ceram Soc 19:2405. doi:10.1016/S0955-2219(99)00129-6
11. Wuchina E, Opeka M, Causey S, Buesking K, Spain J, Cull A, Routbort J, Guitierrez-Mora F (2004) J Mater Sci 39:5939. doi:10.1023/B:JMSC.0000041690.06117.34
12. Ryu HJ, Lee YW, Cha SI, Hong SH (2006) J Nucl Mater 352:341. doi:10.1016/j.jnucmat.2006.02.089
13. Min-Haga E, Scott WD (1988) J Mater Sci 23:2865. doi:10.1007/BF00547460
14. Kim KH, Shim KB (2003) Mater Charact 50:31. doi:10.1016/S1044-5803(03)00055-X
15. Sciti D, Silvestroni L, Bellosi A (2006) J Mater Res 21:1460. doi:10.1557/jmr.2006.0180
16. Sciti D, Silvestroni L, Bellosi A (2006) J Am Ceram Soc 89:2668. doi:10.1111/j.1551-2916.2006.01109.x
17. Silvestroni L, Sciti D (2007) Scripta Mater 57:165. doi:10.1016/j.scriptamat.2007.02.040
18. Anstis GR, Chantikul P, Lawn BR, Marshall DB (1988) J Am Ceram Soc 64:533. doi:10.1111/j.1151-2916.1981.tb10320.x
19. Yan Y, Huang Z, Dong S, Jiang D (2006) J Am Ceram Soc 89:3589. doi:10.1111/j.1551-2916.2006.01270.x
20. German RM (1996) Sintering theory and practice. Wiley, New York
21. Landwehr SE, Hilmas GE, Fahrenholtz WG, Talmy IG (2007) J Am Ceram Soc 90:1998. doi:10.1111/j.1551-2916.2007.01667.x
22. McColm IJ (1990) Ceramic hardness. Plenum Press, New York
23. Taya M, Hayashi S, Kobayashi AS, Yoon HS (1990) J Am Ceram Soc 73:1382. doi:10.1111/j.1151-2916.1990.tb05209.x
24. Shackelford JF, Alexander W (2001) CRC materials science and engineering handbook, 3rd edn. CRC Press, Boca Raton